# Hydrothermal Synthesis of Mesoporous Nanocrystalline Tetragonal $ZrO_2$ Using Dehydroabietyltrimethyl Ammonium Bromine

Peng Wang,*[,a] Zhen-dong Zhao,[b] Zong-de Wang,[a] Shang-xing Chen,[a] and Guo-rong Fan [a]

Mesoporous nanocrystalline tetragonal zirconias were successfully synthesized through a hydrothermal method using a novel bioresource-derived quaternary ammonium salt, dehydroabietyltrimethyl ammonium bromine (DTAB), as a templating agent. The templating agent provides a surface area (242.02 $m^2/g$), high pore volume (0.53 $cm^3/g$), and large average pore diameter (7.65 nm), which suggests that DTAB is a good candidate for mesostructure synthesis. The hydrothermal treatments give the materials improved thermal stabilities because of the generation of tetragonal nanocrystallites that are more stable than the bulk amorphous ones in the hydrothermal process. However, because of the absence of stabilizers, the sizes of the crystallites of the as-synthesized sample increase gradually with increasing calcination temperature. As the crystalline size of the sample rises to 25 nm, the nanocrystallites become too large to integrate well together, causing the well-organized mesostructure to collapse.

*Keywords: Mesoporous; Nanocrystalline materials; Tetragonal zirconia; Rigid quaternary ammonium salt*

*Contact information: a: College of Forestry, Jiangxi Agricultural University, Nanchang, 330045, P.R. China; b: Institute of Chemical Industry of Forestry Products, CAF, Nanjing, 210042, P.R. China;*
** Corresponding author: E-mail: pengwang1981@126.com*

## INTRODUCTION

Since the discovery of ordered mesoporous silica materials through a surfactant-assisted process (Beck *et al.* 1992; Kresge *et al.* 1992), the field of mesoporous materials has been extensively investigated. Zirconias have been receiving much attention due to their great applicability as ceramic materials (Reidy *et al.* 2011), filters or membranes (Qi *et al.* 2012), and catalyst supports (Menegazzo *et al.* 2009). The properties of zirconias largely depend on their textural characteristics, crystalline structures, and grain sizes. Mesoporous zirconias have large Brunauer-Emmett-Teller (BET) surface areas, high pore volumes, and narrow pore-size distributions, making them excellent materials in many applications (Yang *et al.* 1998). Zirconias have three polymorphs: monoclinic, tetragonal, and cubic (Chraska *et al.* 2000; Luo *et al.* 2004). Among them, the tetragonal phase is of particular interest because of the unique bifunctional characteristics of weak acid and basic properties (Yamaguchi 1994) and the high activities in some catalytic reactions (Centi *et al.* 1996).

In contrast to conventional polycrystalline materials, nanocrystalline materials are more promising because of their extremely small crystallite dimensions (Deshmane and Adewuyi 2013). Therefore, it is of great importance to obtain zirconias with high surface

areas and controllable pore structures in their pure tetragonal phase and nanocrystalline frameworks.

Much effort has been devoted to the preparation of mesoporous zirconias using a surfactant-assisted route. By using the cationic surfactant cetyltrimethylammonium bromide (CTAB), Reddy and Sayari (1996) synthesized ordered hexagonal mesoporous $ZrO_2$. Unfortunately, such material was found to be thermally unstable. Ciesla *et al*. (1996) found that the pretreatment with phosphoric acid could improve the thermal stability of the material. After the calcination, the wall composition was 45 wt% zirconium oxide, 54 wt% zirconium phosphate, and 0.5 to 1 wt% zirconium sulfate. However, the phosphate and sulfate group inside the pore wall may restrict the application of this material. Trens and co-workers (1998) reported the synthesis of mesoporous nanocrystalline tetragonal zirconium oxides with high surface areas by using CTAB as a template. They showed that it was possible to control the stacking of the platelets, particle sizes, and stabilities by using surfactants without additional stabilizers. Rezaei *et al.* (2008) demonstrated the preparation of nanocrystalline zirconia powders with high surface areas, mesoporous structures, and tetragonal crystallite phase by using P123 block copolymer surfactant. The addition of surfactant had a significant effect on the structural properties of the zirconias. Nayak *et al*. (2011) introduced the synthesis of ceria-modified mesoporous nanocrystalline tetragonal zirconias by using dodecylamine as a directing agent. The as-synthesized sample possessed a high surface area and large pore volume because of the introduction of the template. Chen and co-workers (2005) showed that hierarchically porous zirconia materials with nanocrystalline frameworks and mesopore structures could be obtained by using composite surfactants of P123 combined with Brij56 as templates. However, mixed tetragonal/monoclinic phases were obtained in the cited study. In the research mentioned above, the surfactant templates played a vital role in the fabrication of mesoporous structures. It is of great significance to pursue new templates for the synthesis of mesoporous materials.

In the present study, a new self-synthesized quaternary ammonium salt, dehydroabietyltrimethyl ammonium bromine (DTAB; Fig. 1), was applied as a structure-directing agent in the synthesis of mesoporous nanocrystalline tetragonal zirconias. Unlike the traditional alkyl-chain surfactants, DTAB possesses a big group of a three-ring phenanthrene skeleton that is rigid and can be a good candidate for the mesostructure synthesis. Moreover, DTAB is derived from biomass feedstocks (rosin). Its low toxicity and renewable properties make it an environmentally friendly reagent for achieving sustainable processes. As far as we know, such a surfactant has not been used for preparing mesoporous nanocrystalline tetragonal zirconias. The effects of surfactant to zirconium molar ratio and calcination temperature were investigated.

## EXPERIMENTAL

### Materials

The $ZrOCl_2 \cdot 8H_2O$ (AR) was purchased from Sinopharm Chemical Reagent Co., Ltd. (China). Sodium hydroxide (AR), formaldehyde (AR), formic acid (AR), and acetone (AR) were provided by Nanjing Chemical Reagent Co., Ltd. (China). Dehydroabietylamine (98%, rosin derivative) was purchased from Hangzhou Wanjing New Materials Co., Ltd. (China).

## Methods

*Synthesis of surfactant*

Dehydroabietyltrimethyl ammonium bromine was synthesized according to Fig. 1. N,N-dimethyl dehydroabietylamine starting from dehydroabietylamine was prepared through the formic acid-formaldehyde method (Pine and Sanchez 1971). Then, dehydroabietyltrimethyl ammonium bromine was synthesized by the reaction of N,N-dimethyl dehydroabietylamine and $CH_3Br$ in acetone. The spectral data were as follows: $^1$H NMR ($CDCl_3$), $\delta$: 1.248 (d, $J$=7.0 Hz, 6 H, C15H-($C\underline{H}_3$)$_2$), 1.282 (s, 3 H, C4-$CH_3$), 1.374 (s, 3 H, C10-$CH_3$), 1.40~2.40 (m, 9 H, C1-$H_2$, C2-$H_2$, C3-$H_2$, C5-H, C6-$H_2$), 2.849 (hept, $J$=7.0 Hz, 1 H, C15$\underline{H}$-($CH_3$)$_2$), 2.915~3.034 (m, 2 H, C7-$H_2$), 3.593 (s, 9 H, ($CH_3$)$_3N^+$), 3.430 (d, $J$=14.0 Hz, 1 H, C18$H_2$-$N^+$), 3.958 (d, $J$=14.0 Hz, 1 H, C18$H_2$-$N^+$), 6.9205 (d, $J$=1.5 Hz, 1 H，C14-H), 7.0128 (dd, $J_1$=1.5 Hz, $J_2$=8.0 Hz, 1 H, C12-H), 7.140 (d, $J$=8.0 Hz, 1 H, C11-H).

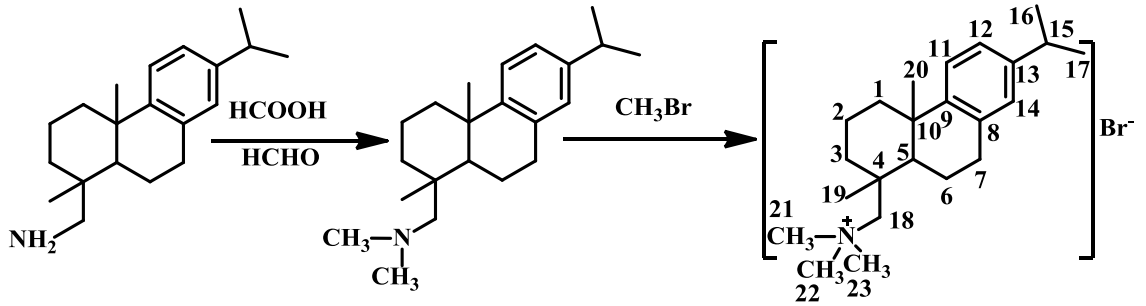


**Fig. 1.** Synthesis route of dehydroabietyltrimethyl ammonium bromine

*Preparation of materials of $ZrO_2$*

In a typical preparation, 0.02 mol of $ZrOCl_2 \cdot 8H_2O$ and a set amount of DTAB (surfactant to zirconium molar ratio: 0.025, 0.05, 0.075, or 0.1) were dissolved in 30 mL of deionized water at 70 °C. Then, 30 mL of an aqueous solution containing NaOH (0.1 mol) was then added while stirring. After further stirring for 4 h, the precipitated products were transferred into a Teflon-lined autoclave and heated at 100 °C for 24 h. The products were washed with water and ethanol several times to remove sodium ions and unbound surfactant. After drying at 50 °C under vacuum for 12 h, the templating agents were removed by calcination at 450 °C, 550 °C, and 650 °C for 2 h at the rate of 1 °C/min. The results are denoted Zr-X-Y, where Zr represents zirconia, X represents the molar ratio of DTAB to zirconium, and Y represents the calcination temperature.

*Characterization*

The crystalline phases of the samples were recorded by an X-ray diffractometer (XRD; D8 Focus, Bucker AXS Inc., Germany) with Cu Ka radiation ($k$ = 0.154 nm). The operating target voltage was 40 kV and the current was 40 mA. The sample was powdered and scanned at 2$\theta$ ranging from 0.5 to 10.0º for small-angle and 20.0 to 80.0º for large-angle. Transmission electron microscopy (TEM) images were obtained with a JEOL JEM-2100 (Japan) instrument operated at an accelerating voltage of 200 kV. The samples were ultrasonically dispersed in ethanol and then dropped onto carbon-coated copper grids prior to the measurements. Porosity and surface area measurements were performed following the $N_2$ adsorption on a Micromeritics ASAP2020 instrument (Micromeritics Instrument Corp., USA). The surface areas were calculated using the Brunauer-Emmett-Teller (BET) model (Brunauer *et al.* 1938). Average pore diameters

were calculated using the Barrett-Joyner-Halenda (BJH) method (Barrett *et al.* 1951) from the desorption branch of isotherm. Thermogravimetry and differential scanning calorimetry (TGA-DSC) were performed on a NETZSCH STA409PC (Netzsch Ltd. Corp., Germany) thermogravimetric analyzer from 60-1000 ºC with a heating rate of 10 ºC/min in air (20 mL/min). $^1$H NMR spectra was recorded using Bruker AV500 NMR spectrometer (Bucker AXS Inc., Germany). Prior to the measurement, DTAB was dissolved in $CDCl_3$.

## RESULTS AND DISCUSSION

### Effects of DTAB Dosages on the Microstructure Characteristics of $ZrO_2$

Figure 2 shows the small-angle XRD patterns of the as-synthesized samples. All of the samples exhibited a broad diffraction peak in the 2$\theta$ range from 1.14° ($d_{100}$=7.74 nm) to 1.33° ($d_{100}$=6.64 nm), indicating the existence of a well-organized 3D wormhole mesoporous structures without a long range order (Tanev and Pinnavaia 1995). With increasing DTAB dosage, the intensity of the diffraction peaks first increased and then decreased, which demonstrates that only the suitable dosage of DTAB was able to enhance the regularity of the pore structures. When the DTAB dosage was small, the low concentrate of DTAB was not sufficient to induce the co-assembly of zirconium species to form regular structure. However, when the DTAB dosage was too large, the high concentrate of DTAB left insufficient space for the zirconium species to assemble on the surface of the DTAB micelles.

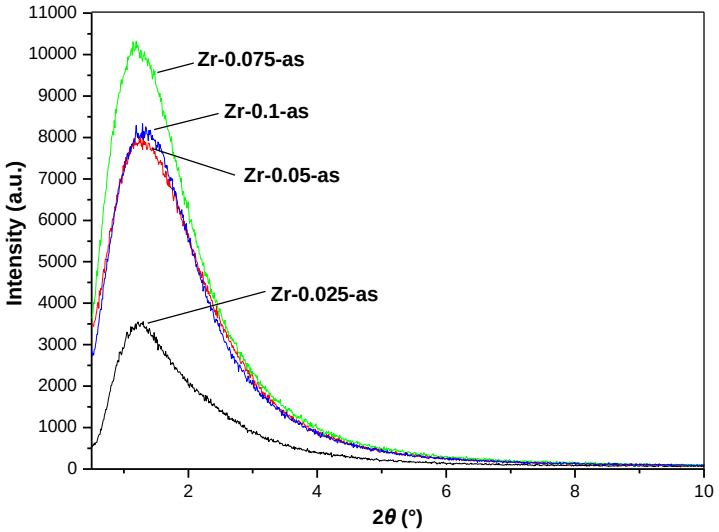


**Fig. 2.** Small-angle XRD patterns of as-synthesized tetragonal nanocrystalline mesoporous $ZrO_2$ synthesized with different DTAB dosages

Large-angle XRD patterns for the as-synthesized samples are shown in Fig. 3. All of the samples showed five peaks, at 2$\theta$=30.26°, 2$\theta$=35.21°, 2$\theta$=50.58°, 2$\theta$=60.21°, and 2$\theta$=74.65°, which can be related to the diffraction peaks of the tetragonal phase. The Scherrer equation (Patterson 1939) was applied to calculate crystalline sizes. The results showed that the crystalline sizes of the as-synthesized samples were about 5.4 nm. After precipitation by NaOH, hydrothermal treatment is employed. Because the hydrated zirconium hydroxides are not stable in the hydrothermal condition, the samples became

dehydrated and turned into zirconias. In a strongly alkaline environment, the resultant zirconias begin to crystallize gradually, and they finally become transformed into nanocrystalline tetragonal zirconias. The patterns of the samples synthesized with different DTAB dosages were similar, which indicates that the DTAB dosages had no effect on the internal crystal structures of the materials.

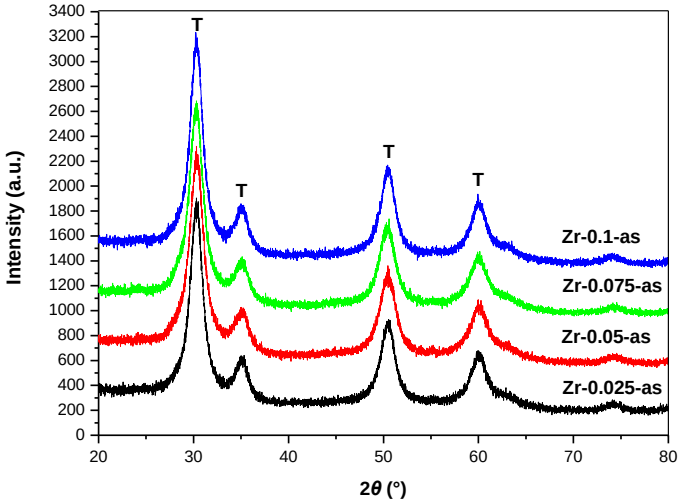


**Fig. 3.** Large-angle XRD patterns of as-synthesized tetragonal nanocrystalline mesoporous $ZrO_2$ synthesized with different DTAB dosages

Figure 4 shows the small-angle XRD patterns of the calcined samples. All of the samples showed a distinct diffraction peak in the $2\theta$ range from 0.83° ($d_{100}$=10.63 nm) to 1.13° ($d_{100}$=7.74 nm), indicating the perseveration of well-organized mesoporous structures in the samples after calcination. Because of the removal of the surfactants, the shape of the peaks became sharper and their intensity stronger. The small-angle peaks of the calcined samples shifted to lower angles, which can be related to the growth of zirconia nanocrystallites.

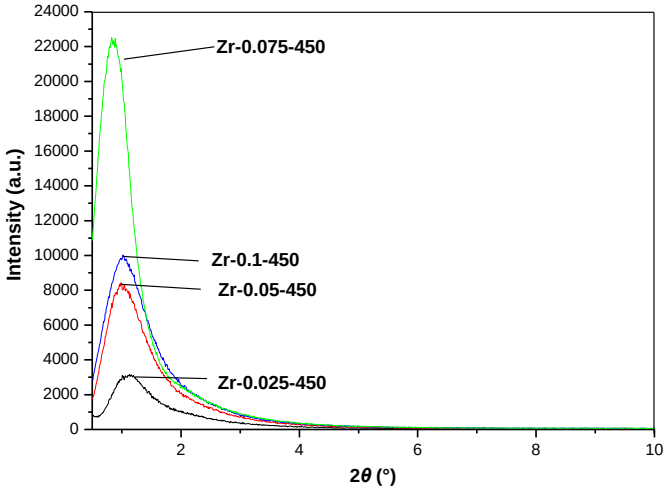


**Fig. 4.** Small-angle XRD patterns of calcined tetragonal nanocrystalline mesoporous $ZrO_2$ synthesized with different DTAB dosages

As can be seen from Fig. 5, all of the calcined samples showed the typical diffraction peaks of the tetragonal zirconia phase. In comparison to the as-synthesized

samples, the intensity and shape of the diffraction peaks of the calcined samples became stronger and sharper, which indicates that the calcination can improve the crystallinity. According to the Scherrer formula (Patterson 1939), the crystalline sizes of the calcined samples were about 6.2 nm, suggesting that calcination increased the crystallite size.

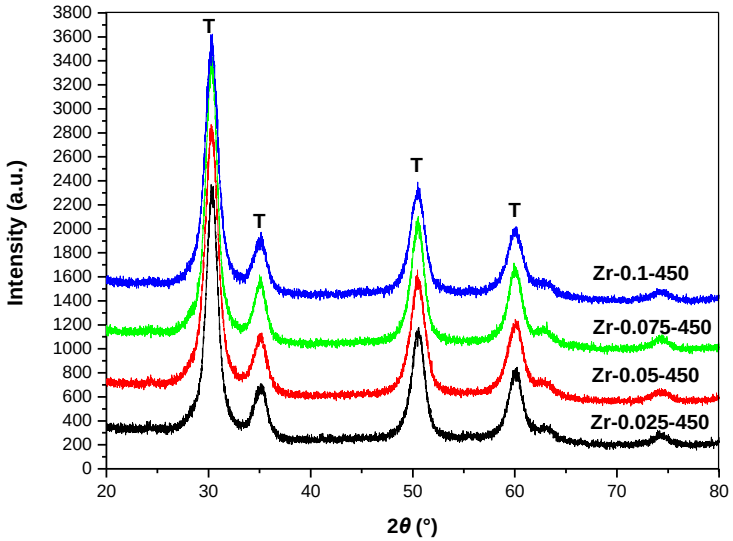


**Fig. 5.** Large-angle XRD patterns of calcined tetragonal nanocrystalline mesoporous $ZrO_2$ synthesized with different DTAB dosages

As shown in Fig. 6, all of the samples exhibited distinct IV type isotherms with large hysteresis loops, indicating the existence of mesoporous frameworks. The BJH analyses of desorption branches are illustrated in Fig. 7. All of the samples reveal narrow single peak distributions. Sample Zr-0.05-450 possessed a larger mesopore than the other samples, concentrating at 12.75 nm. Table 1 summarizes the textural properties of the calcined samples. All of the samples had specific surface areas larger than 120 $m^2/g$. The surface area, pore volume, and average pore diameter reached their respective maximum values as the DTAB to zirconium molar ratio reached 0.05.

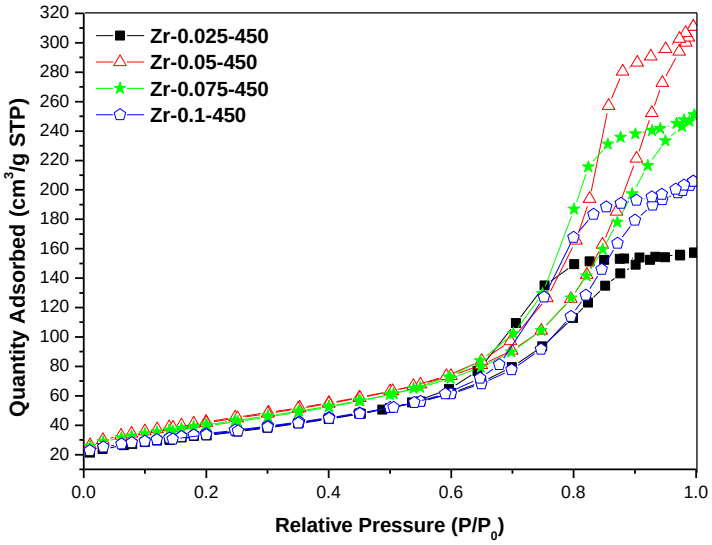


**Fig. 6.** $N_2$ adsorption-desorption isotherms of calcined tetragonal nanocrystalline mesoporous $ZrO_2$ synthesized with different DTAB dosages

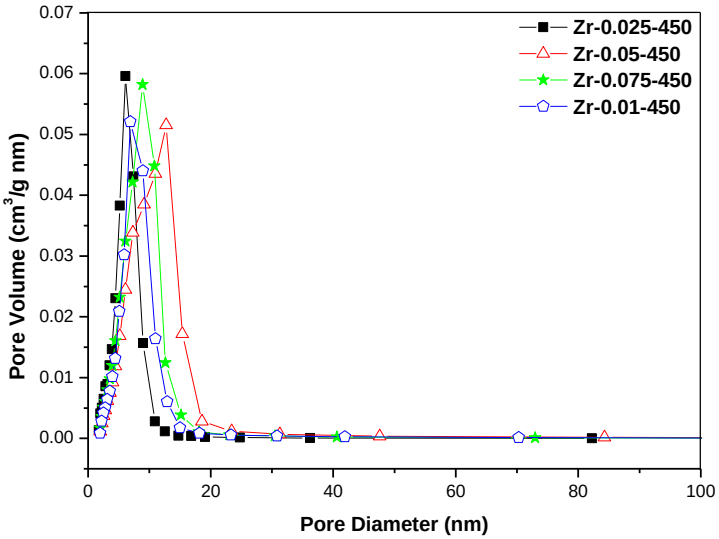


**Fig. 7.** BJH pore size distributions of calcined tetragonal nanocrystalline mesoporous $ZrO_2$ synthesized with different DTAB dosages

**Table 1.** Textural Properties of Calcined Tetragonal Nanocrystalline Mesoporous $ZrO_2$ Synthesized with Different DTAB Dosages

| Sample | $S_{BET}$ ($m^2$/g) | V ($cm^3$/g) | D (nm) |
|---|---|---|---|
| Zr-0.025-450 | 121.92 | 0.25 | 6.06 |
| Zr-0.05-450 | 152.92 | 0.48 | 9.89 |
| Zr-0.075-450 | 145.11 | 0.39 | 8.1 |
| Zr-0.1-450 | 122.79 | 0.32 | 7.66 |
| $S_{BET}$: surface area; V: pore volume; and D: average pore diameter | | | |

## Effects of Calcinations on the Microstructural Characteristics of $ZrO_2$

Figure 8 illustrates the small-angle XRD patterns of the samples calcined at different temperatures. Sample Zr-0.05-as shows a broad small-angle diffraction peak at $2\theta$=1.24° ($d_{100}$=7.12 nm). After calcination at 450 °C, the small-angle peak became sharper and stronger because of the removal of surfactants. At the same time, the peak shifted to a smaller $2\theta$ value of 1.08° ($d_{100}$=8.17 nm) because of the growth of zirconia nanocrystallites. As the calcination temperature increased to 550 °C, the intensity of the peak decayed, indicating that further increasing the calcination temperature can lead to a decrease in pore structure regularity. The peak shifted to a much smaller $2\theta$ value of 0.98° ($d_{100}$=9.01 nm), suggesting the further growth of zirconia nanocrystallites. With calcination temperature increasing to 650 °C, the peak almost disappeared, which implies there was damage to the mesoporous structure.

As shown in Fig. 9, as the calcination temperature increased, the diffraction peaks that can be related to the tetragonal phase became sharper. This result suggests again that an increase in calcination temperature can lead to an increase in the crystallinity. According to the Scherrer formula (Patterson 1939), the crystalline size of the sample calcined at 550 °C was about 9.1 nm, implying the further increase of the crystallites caused by higher calcination temperature. With calcination temperature increasing to 650 °C, the diffraction peaks at $2\theta$=28.24° and $2\theta$=31.49°, belonging to the monoclinic phase,

began to appear, indicating the phase transformation from the tetragonal phase into the monoclinic phase formed by the excessively high calcination temperature.

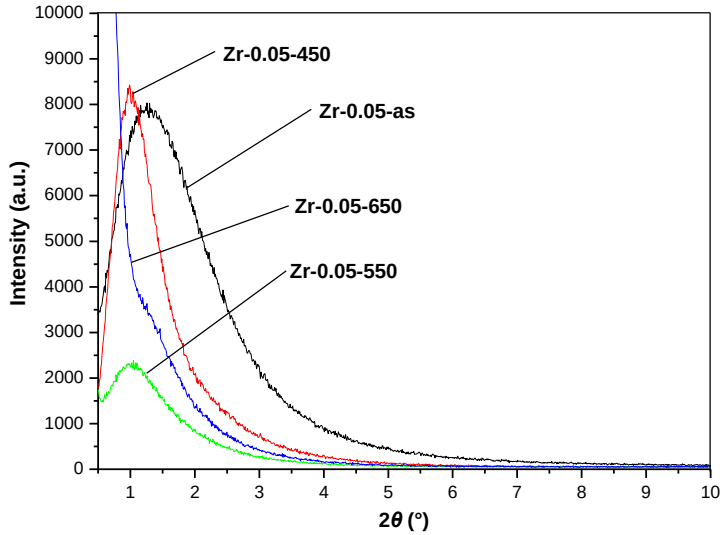


**Fig. 8.** Small-angle XRD patterns of tetragonal nanocrystalline mesoporous $ZrO_2$ calcined at various temperatures

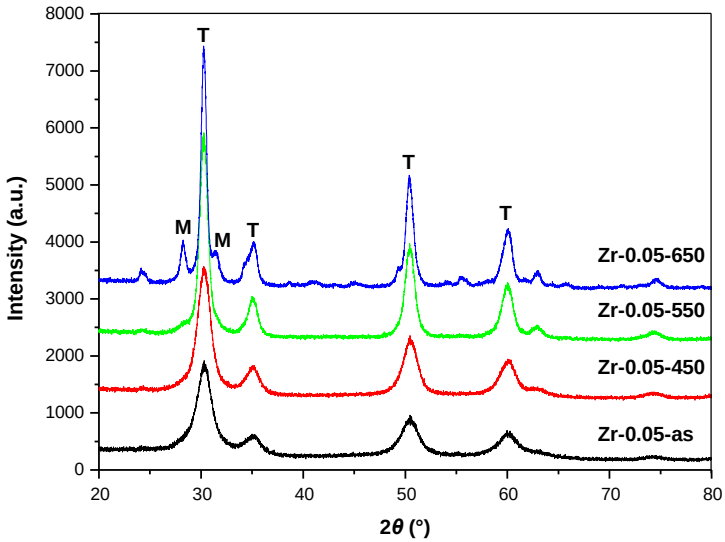


**Fig. 9.** Large-angle XRD patterns of tetragonal nanocrystalline mesoporous $ZrO_2$ calcined at various temperatures

Figure 10 depicts the $N_2$ adsorption-desorption isotherms of the samples calcined under different temperatures. The samples Zr-0.05-as, Zr-0.05-450, and Zr-0.05-550 show typical IV type isotherms, suggesting the presence of mesoporous structures. With increasing calcination temperature, the hysteresis loops shifted to higher relative pressure values, suggesting the broadening of pore size distributions. The sample Zr-0.05-650 shows a V-type isotherm, indicating the collapse of the well-organized mesoporous structure. The as-synthesized sample shows a narrow BJH mesopore size distribution concentrating at about 10 nm, as can be seen in Fig. 11. With increasing calcination temperature, the pore size of the samples became marginally larger and the pore distributions became slightly broader.

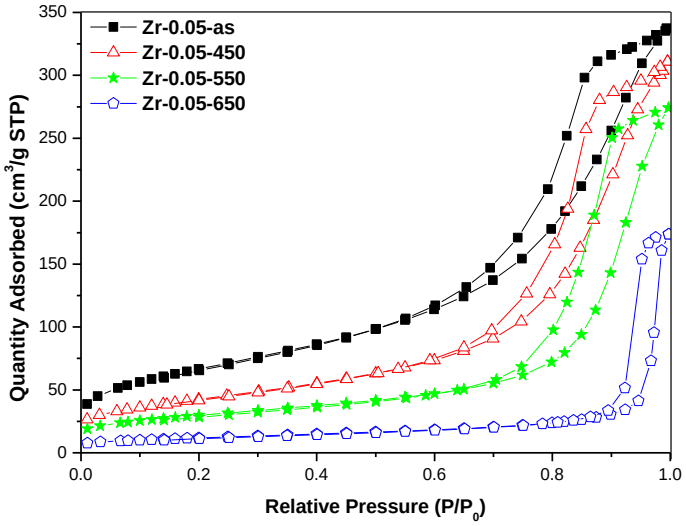


**Fig. 10.** $N_2$ adsorption-desorption isotherms of tetragonal nanocrystalline mesoporous $ZrO_2$ calcined at various temperatures

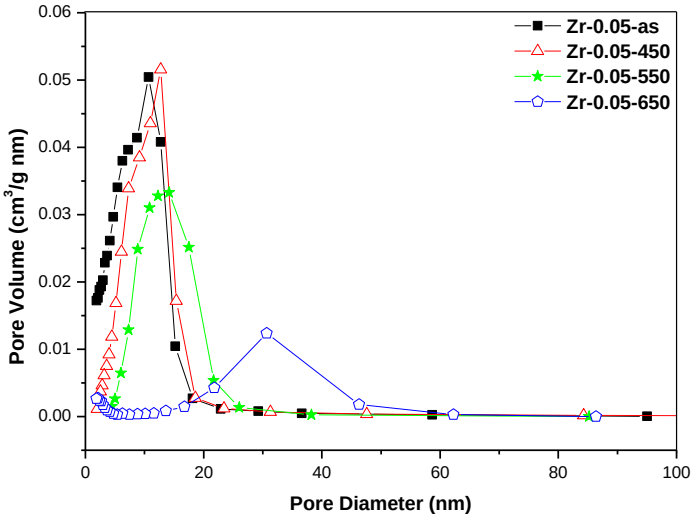


**Fig. 11.** BJH pore size distributions of tetragonal nanocrystalline mesoporous $ZrO_2$ calcined at various temperatures

**Table 2.** Textural Properties of Tetragonal Nanocrystalline Mesoporous $ZrO_2$ Calcined at Various Temperatures

| Sample | $S_{BET}$ ($m^2$/g) | V ($cm^3$/g) | D (nm) |
|---|---|---|---|
| Zr-0.05-as | 242.02 | 0.53 | 7.65 |
| Zr-0.05-450 | 152.92 | 0.48 | 9.89 |
| Zr-0.05-550 | 107.34 | 0.43 | 12.96 |
| Zr-0.05-650 | 42.57 | 0.27 | 24.78 |
| $S_{BET}$: surface area; V: pore volume; and D: average pore diameter | | | |

As the calcination temperature was increased to 650 °C, the broadest pore size distribution formed, ranging from 2 nm to 60 nm, because of the damage of the mesoporous structure. The textural properties of the samples calcined under different temperatures are summarized in Table 2. The as-synthesized sample had a large surface

area (242.02 $m^2$/g), high pore volume (0.53 $cm^3$/g), and large average pore diameter (7.65 nm), which suggests that DTAB is a good candidate for mesostructure synthesis. The calcination temperature exerts a negative effect on the surface area and pore volume and a positive effect on the pore sizes of the samples. When the calcination temperature reached 650 °C, the surface area of sample Zr-0.05-650 deceased sharply to 42.57 $m^2$/g because of the destruction of the mesoporous structure.

Figure 12 shows TEM images of the samples calcined at various temperatures.

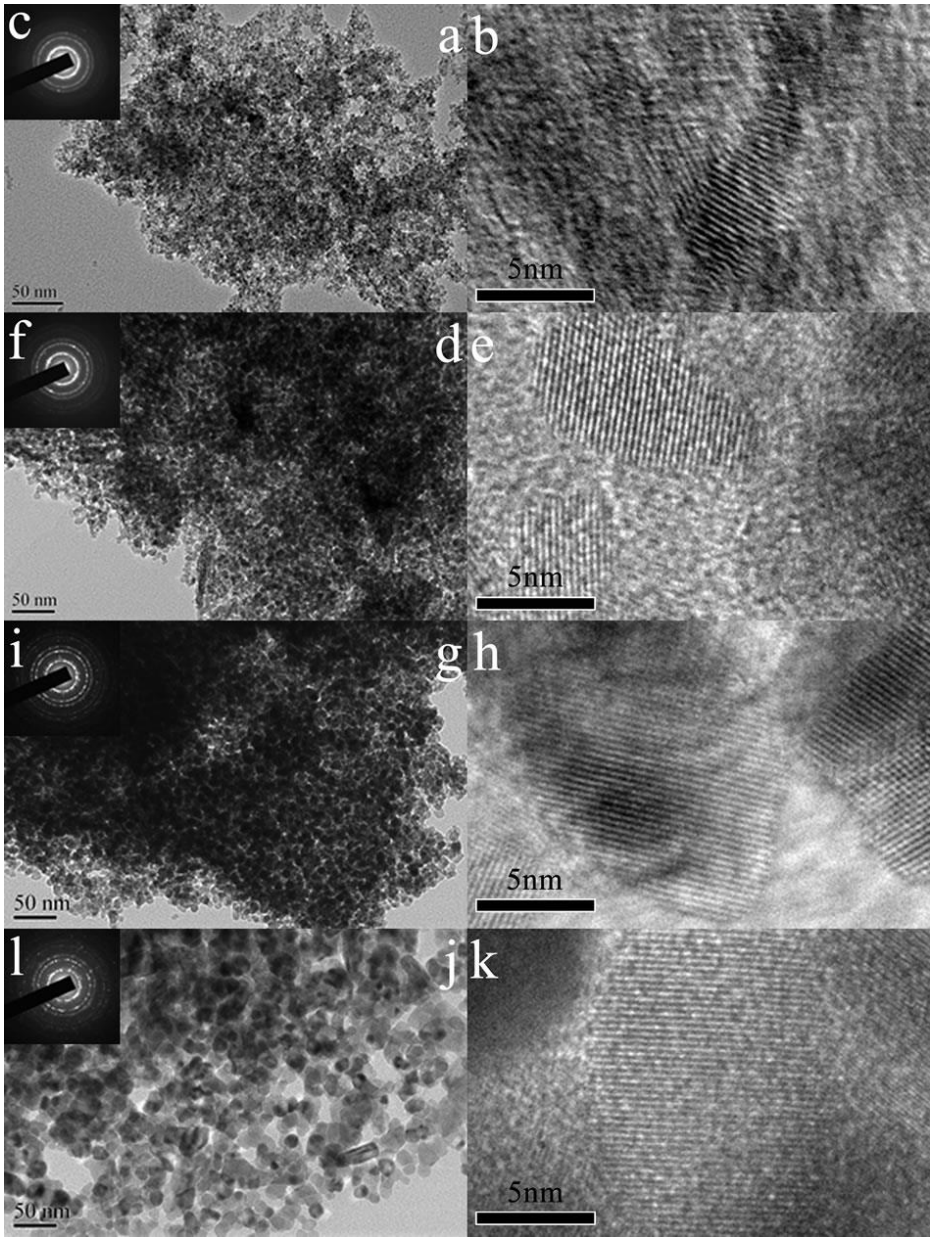


**Fig. 12.** TEM images of tetragonal nanocrystalline mesoporous $ZrO_2$ calcined under different temperatures. (a), (b), and (c): typical image, high-resolution TEM and electron diffraction pattern of sample Zr-0.05-as; (d), (e), and (f): typical image, high-resolution TEM and electron diffraction pattern of sample Zr-0.05-450; (g), (h), and (i): typical image, high-resolution TEM and electron diffraction pattern of sample Zr-0.05-550; and (j), (k), and (l): typical image, high-resolution TEM and electron diffraction pattern of sample Zr-0.05-650

As shown in Figs. 12a and 12b, the pore wall of the as-synthesized sample was fully composed of zirconia nanocrystallites, which was closely integrated to form a well-organized mesoporous structure. The crystalline size in the TEM image was about 6 nm. As the calcination temperature increased, the crystalline sizes of the samples Zr-0.05-450 (Figs. 12d and 12e) and Zr-0.05-550 (Figs. 12g and 12h) increased to 8 nm and 11 nm, respectively. These results were slightly larger than those calculated by the Scherrer formula. The nanocrystallites of the two samples were still closely integrated to preserve the well-organized mesoporous structures. As the calcination temperature was increased to 650 °C, the crystalline size of the sample rose to 25 nm, which is too large to maintain their well-integrated nature, causing the well-organized mesostructures to collapse. This result is similar to the work of Hung *et al.* (2008). The resulting pore structure of the sample was merely obtained from the simple accumulation of nanocrystallites. That is why sample Zr-0.05-650 possessed rather poor textural properties. Figures 12c, 12f, and 12i show the electron diffraction patterns obtained from selected areas, suggesting that tetragonal zirconias were formed in the samples. As the calcination temperature increased, the diffraction rings became clearer, indicating an increase in the crystallinities. In Fig. 12l, additional vague diffraction rings can be observed, indicating the existence of mixed tetragonal/monoclinic phases. The as-synthesized sample had great thermal stability because of the existence of tetragonal nanocrystallites, which are more stable than the bulk amorphous ones (Trens *et al.* 1998 ). However, because of the absence of stabilizers, the crystallites of the samples grow gradually as the calcination temperature increases, until the well-organized mesostructure finally collapses.

Figure 13 plots the TGA–DSC curve of as-synthesized sample Zr-0.05-as. The DSC curve presents three major peaks, in which one is endothermic and the other two are exothermic. The first peak appearing at 106 °C can be related to the elimination of residual water, with a weight loss of about 6 % in the AB region. The second one at about 339 °C is due to the decomposition of the organic templating agent DTAB, with a weight loss of about 2.5 % in the BC region. The last one at 440 °C corresponds to the removal of hydroxyl groups bonded on the surface of zirconia that were not completely removed by dehydration during the hydrothermal treatment, with a weight loss of about 2 % in the CD region.

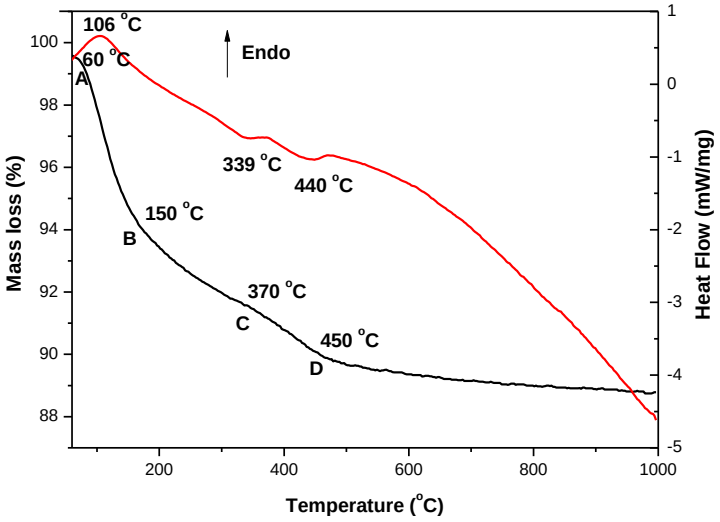


**Fig. 13.** TGA-DSC curve of as-synthesized tetragonal nanocrystalline mesoporous $ZrO_2$ (Zr-0.05-as)

**Table 2.** Comparison of Experimental Conditions and the Results of Prior Studies with Present Work

| Zirconium source | Templating agent | Pretreatment or Stabilizer | pH | Calcination temperature (°C) | Particle size (nm) | Surface area ($m^2$/g) | Pore size (nm) | Pore volume ($cm^3$/g) | Reference |
|---|---|---|---|---|---|---|---|---|---|
| $ZrOCl_2$ | CTAB | Refluxing 90h | 11.6 | 500 | <10 | 326 | 7 | 0.56 | Trens *et al.* 1998 |
| $ZrO(NO_3)_2$ | P123 | Refluxing 24h 80 °C | 11 | 600 | 8.8 | 136.88 | 4 | 0.177 | Rezaei *et al*. 2008 |
| $Zr(NO_3)_4$ | P123 | Refluxing 24h 80 °C | 11 | 600 | 9.8 | 128.5 | 5.39 | 0.219 | Rezaei et al. 2008 |
| $ZrOCl_2$ | P123 | Refluxing 24h 80 °C | 11 | 600 | 9.1 | 138.23 | 11.32 | 0.44 | Rezaei et al. 2008 |
| $ZrOCl_2$ | dodecylamine | $(NH_4)_2Ce(NO_3)_6$ | 8.5 | 500 | 10 | 80 | 7 | 0.07 | Nayak *et al*. 2011 |
| $Zr(OC_3H_7)_4$ | P123+Brij56 | Hydrothermal treatment 12h 130 °C | - | 500 | 5 | 91 | 4.7, 20~60, 250~500* | 0.21 | Chen *et al.* 2005 |
| $ZrOCl_2$ | - | Refluxing 96h 102 °C | 11 | 600 | 2.78 | 343.5 | 3.9 | 0.335 | Deshmane *et al*. 2013 |
| $ZrOCl_2$ | DTAB | Hydrothermal treatment 24h 100 °C | 12 | 450 | 8.0 | 152.92 | 9.89 | 0.48 | Present work |
| * means hierarchically porous structure | | | | | | | | | |

Table 2 lists the comparison of experimental conditions and the results of prior studies with the present work. As for the pore size, the introductions of the templating agents can significantly enlarge the pore sizes of the resulted materials. In contrast to the other works, especially the work of Trens *et al*. (1998), the zirconia obtained in the present work possessed a larger pore size, and at the same time, large surface area and high pore volume. The resulting larger pore size was contributed by the templating agent DTAB and the hydrothermal treatment. Trens *et al.* (1998) found that longer times of refluxing in high concentration basic environment could improve the thermal stability of the materials, because the nanosized semicrystalline zirconias were formed. Deshmane *et al*. 2013) obtained similar conclusions. The improved thermal stability can be related to the slight unit cell shrinkage of nanosized semicrystalline zirconias in calcination, while the amorphous solids suffer strong unit cell shrinkage which will decrease the pore sizes of the materials, and destroy the mesoporous structures. In order to eliminate the effect unit cell shrinkage, a strong basic environment (pH = 12) and hydrothermal treatment were used to synthesize nanosized fully crystalline zirconias in the pretreatment process. Therefore, without the unit cell shrinkage a larger pore size was obtained, and at the same time large surface area and high pore volume were maintained.

## CONCLUSIONS

1. A bioresource-derived quaternary ammonium salt, dehydroabietyltrimethyl ammonium bromine, was applied as templating agent for the synthesis of mesoporous nanocrystalline tetragonal $ZrO_2$.
2. When the templating agent to zirconium molar ratio was 0.05, the as-synthesized sample exhibited a large surface area (242.02 $m^2$/g), a high pore volume (0.53 $cm^3$/g), and a large average pore diameter (7.65 nm), which suggests that DTAB is a good candidate for the mesostructure synthesis.
3. After the hydrothermal treatment, the as-synthesized sample was fully composed of zirconia nanocrystallites, which were closely integrated to form a well-organized

mesoporous structure. Such samples have great thermal stability because of the generation of tetragonal nanocrystallites, which are more stable than the bulk amorphous ones in the hydrothermal process. However, because of the absence of stabilizers, the crystallites of the samples grew as the calcination temperature increased. As the calcination temperature climbed to 650 °C, the crystalline size of the sample increased to 25 nm, which is too large to stay well-integrated, causing the well-organized mesostructures to collapse.

## ACKNOWLEDGMENTS

This work was supported by the Research Fund for the Doctoral Program of Higher Education of China (Grant No. 20133603120002).

## REFERENCES CITED

Barrett, E. P., Joyner, L. G., and Halenda, P. P. (1951). "The determination of pore volume and area distributions in porous substances. I. Computations from nitrogen isotherms," *Journal of the American Chemical Society* 73(1), 373-380. DOI: 10.1021/ja01145a126

Beck, J., Vartuli, J., Roth, W., Leonowicz, M., Kresge, C., Schmitt, K., Chu, C., Olson, D., and Sheppard, E. (1992). "A new family of mesoporous molecular sieves prepared with liquid crystal templates," *Journal of the American Chemical Society* 114(27), 10834-10843. DOI: 10.1021/ja00053a020

Brunauer, S., Emmett, P. H., and Teller, E. (1938). "Adsorption of gases in multimolecular layers," *Journal of the American Chemical Society* 60(2), 309-319. DOI: 10.1021/ja01269a023

Centi, G., Cerrato, G., D'Angelo, S., Finardi, U., Giamello, E., Morterra, C., and Perathoner, S. (1996). "Catalytic behavior and nature of active sites in copper-on-zirconia catalysts for the decomposition of $N_2O$," *Catalysis Today* 27(1-2), 265-270. DOI: 10.1016/0920-5861(95)00197-2

Chen, H., Gu, J., Shi, J., Liu, Z., Gao, J., Ruan, M., and Yan, D. (2005). "A composite surfactant route for the synthesis of thermally stable and hierarchically porous zirconia with a nanocrystallized framework," *Advanced Materials* 17(16), 2010-2014. DOI: 10.1002/adma.200500221

Chraska, T., King, A. H., and Berndt, C. C. (2000). "On the size-dependent phase transformation in nanoparticulate zirconia," *Materials Science and Engineering: A* 286(1), 169-178. DOI: 10.1016/S0921-5093(00)00625-0

Ciesla, U., Schacht, S., Stucky, G. D., Unger, K. K., and Schüth, F. (1996). "Formation of a porous zirconium oxo phosphate with a high surface area by a surfactant‐assisted synthesis," *Angewandte Chemie International Edition in English* 35(5), 541-543. DOI: 10.1002/anie.199605411

Deshmane, V. G., and Adewuyi, Y. G. (2013). "Mesoporous nanocrystalline sulfated zirconia synthesis and its application for FFA esterification in oils," *Applied Catalysis A: General* 462-463, 169-206. DOI: 10.1016/j.apcata.2013.05.005

Hung, I., Fung, K.-Z., Hung, D.-T., and Hon, M.-H. (2008). "Thermal stability of ordered mesoporous yttria-stabilized zirconia," *Journal of the European Ceramic Society* 28(6), 1161-1167. DOI: 10.1016/j.jeurceramsoc.2007.09.044

Kresge, C., Leonowicz, M., Roth, W., Vartuli, J., and Beck, J. (1992). "Ordered mesoporous molecular sieves synthesized by a liquid-crystal template mechanism," *Nature* 359(6397), 710-712. DOI: 10.1038/359710a0

Luo, T., Liang, T., and Li, C. (2004). "Stabilization of cubic zirconia by carbon nanotubes," *Materials Science and Engineering: A* 366(1), 206-209. DOI: 10.1016/j.msea.2003.09.053

Menegazzo, F., Pinna, F., Signoretto, M., Trevisan, V., Boccuzzi, F., Chiorino, A., and Manzoli, M. (2009). "Quantitative determination of sites able to chemisorb CO on $Au/ZrO_2$ catalysts," *Applied Catalysis A: General* 356(1), 31-35. DOI: 10.1016/j.apcata.2008.12.004

Nayak, P., Nayak, B. B., and Mondal, A. (2011). "Surfactant assisted synthesis of high surface area ceria modified mesoporous tetragonal zirconia powder and its chromium adsorption study," *Materials Chemistry and Physics* 127(1), 12-15. DOI: 10.1016/j.matchemphys.2011.01.031

Patterson, A. (1939). "The Scherrer formula for X-ray particle size determination," *Physical Review* 56(10): 978. DOI: 10.1103/PhysRev.56.978-982

Pine, S. H., and Sanchez, B. L. (1971). "Formic acid-formaldehyde methylation of amines," *The Journal of Organic Chemistry* 36(6), 829-832. DOI: 10.1021/jo00805a022

Qi, H., Zhu, G., Li, L., and Xu, N. (2012). "Fabrication of a sol-gel derived microporous zirconia membrane for nanofiltration," *Journal of Sol-Gel Science and Technology* 62(2), 208-216. DOI: 10.1007/s10971-012-2711-0

Reddy, J. S., and Sayari, A. (1996). "Nanoporous zirconium oxide prepared using the supramolecular templating approach," *Catalysis Letters* 38(3-4), 219-223. DOI: 10.1007/BF00806572

Reidy, C. J., Fleming, T. J., Hampshire, S., and Towler, M. R. (2011). "Comparison of microwave and conventionally sintered yttria-doped zirconia ceramics," *International Journal of Applied Ceramic Technology* 8(6), 1475-1485. DOI: 10.1111/j.1744-7402.2011.02608.x

Rezaei, M., Alavi, S., Sahebdelfar, S., and Yan, Z.-F. (2008). "Effect of process parameters on the synthesis of mesoporous nanocrystalline zirconia with triblock copolymer as template," *Journal of Porous Materials* 15(2), 171-179. DOI: 10.1007/s10934-007-9120-8

Tanev, P. T., and Pinnavaia, T. J. (1995). "A neutral templating route to mesoporous molecular sieves," *Science* 267(5199), 865-867. DOI: 10.1126/science.267.5199.865

Trens, P., Hudson, M. J., and Denoyel, R. (1998). "Formation of mesoporous, zirconium (IV) oxides of controlled surface areas," *Journal of Materials Chemistry* 8(9), 2147-2152. DOI: 10.1039/A805193C

Yamaguchi, T. (1994). "Application of $ZrO_2$ as a catalyst and a catalyst support," *Catalysis Today* 20(2), 199-217. DOI: 10.1016/0920-5861(94)80003-0

Yang, P., Zhao, D., Margolese, D. I., Chmelka, B. F., and Stucky, G. D. (1998). "Generalized syntheses of large-pore mesoporous metal oxides with semicrystalline frameworks," *Nature* 396(6707), 152-155. DOI: 10.1038/24132

Article submitted: October 29, 2014; Peer review completed: December 11, 2014; Revised version received and accepted: December 18, 2014; Published: January 6, 2015.